

03,08

Optical and spin properties of silicon vacancy centers created by proton irradiation in a 6H/15R silicon carbide heterostructure

© I.A. Eliseyev, E.V. Edinach, O.P. Kazarova, A.N. Smirnov[¶]

Ioffe Institute,
St. Petersburg, Russia

[¶] E-mail: alex.smirnov@mail.ioffe.ru

Received April 28, 2023

Revised April 28, 2023

Accepted April 30, 2023

Optically active silicon vacancy defects (V_{Si}) with an electron spin $S = 3/2$ in a 6H-SiC/15R-SiC silicon carbide heterostructure grown by high-temperature sublimation technique have been studied. By means of low-temperature micro-photoluminescence (μ -PL) and electron paramagnetic resonance (EPR) techniques, we demonstrate the potential to generate five disparate types of V_{Si} centers with distinct spectral properties in the aforementioned heterostructure using proton irradiation with $E = 15$ MeV. Wherein each type of V_{Si} center is defined by its zero-phonon line (ZPL) and a distinct value of spin sublevel splitting in a zero magnetic field. As a result, we have demonstrated the scalability of the number of optically active spin centers that can be enclosed within a single crystalline matrix.

Keywords: silicon carbide, heterostructures, photoluminescence, electron paramagnetic resonance, proton irradiation, spin centers.

DOI: 10.21883/PSS.2023.06.56112.74

1. Introduction

High-spin states of optically active defects in wide-band semiconductors are currently considered to be one of the main platforms for quantum technology development [1–4]. The main property of defects enabling them to be used in quantum technologies is in the fact that the zero-field split (ZFS) high-spin state of a defect may be optically polarized due to the presence of a spin-dependent recombination channel in the optical defect excitation cycle [1–4]. Silicon carbide (SiC) vacancy defects having the ability of optically-induced alignment of spin sublevels in the ground state are among the most prominent representatives of such defects [2,4–6]. Such defects may be conveniently divided into two wide classes: pair defects having a triplet ($S = 1$) ground state [5,7–9] and vacancy defects having a quadruplet ($S = 3/2$) ground state [4–6]. The triplet defects are most prominently represented by negatively charged $V_{\text{Si}}-V_{\text{C}}$ divacancies (nearest pair of silicon and carbon vacancies) [5,7] and negatively charged nitrogen vacancy complexes ($\text{N}_{\text{C}}-V_{\text{Si}}$) [8,9]. Defects based on negatively charged silicon vacancy (V_{Si}) are optically-active centers with spin $S = 3/2$ [4–6]. It should be noted that currently there is no generally accepted microscopic model of defects with spin $S = 3/2$. Some studies address this defect as an isolated silicon vacancy [10]. Other studies address the same centers as a negatively charged silicon vacancy excited by a carbon vacancy in a neutral charge state or by a nonparamagnetic impurity with each of them being molecularly non-coupled with the silicon vacancy [5,11]. To avoid confusion, optically-active centers with spin $S = 3/2$ will be designated hereinafter using a generally accepted

abbreviation of their zero phonon luminescence line (ZPL) and spin sublevel splitting $S = 3/2$ in a zero magnetic field $2D$, where the D parameter is the fine structure constant [6,11]. This data is listed in the Table for SiC polytypes 6H and 15R. It should be noted that SiC polytypism is an additional degree of freedom allowing to control spin and optical properties of defects which is illustrated by defects listed in the Table.

The objective of this study is to demonstrate whether optically-active V_{Si} centers with $S = 3/2$ can be formed in SiC heterostructures through the radiation defect engineering technology and to demonstrate whether optically-induced inverse population of spin sublevels of V_{Si} centers can be formed in these heterostructures. The latter is the main criterion of defect spin state suitability for quantum technologies. For this, confocal micro Raman spectroscopy, microphotoluminescence (μ -PL) and electron paramagnetic resonance (EPR) methods were used to investigate 6H-SiC/15R-SiC heterostructure grown by the sublimation sandwich method [12]. The investigations have shown that optically-addressable V_{Si} centers with spin $S = 3/2$ may be used in such heterostructure.

2. Experimental

6H-SiC/15R-SiC heterostructures were grown in a resistive heating unit using a modified high-temperature gas-phase sublimation (PVT) method — sublimation sandwich method [12]. 6H polytype silicon carbide with high structural perfection and purity ($N_d - N_a \approx 5 \cdot 10^{16} \text{ cm}^{-3}$) was used as a seed crystal. 15R polytype SiC crystal growth

Designations of optically-active V_{Si} centers with $S = 3/2$ in 6H-SiC and 15R-SiC, energies and wavelengths of corresponding ZPL, zero-field splitting (2D) including the sign of fine structure constant D

| Polytype | 6H-SiC | | | 15R-SiC | | |
|---------------------|-----------|-----------|-----------|-------------|-----------|-------------|
| | ZPL | V1 | V2 | V3 | V2 | V3 |
| $E, eV/\lambda, nm$ | 1.433/865 | 1.397/887 | 1.368/906 | 1.399/886.5 | 1.372/904 | 1.352/917.4 |
| ZFS (2D), MHz | -27 | +128 | -27 | +139 | -11.6 | +16.7 |

temperature was within 2000–2100°C, argon pressure in the growth vessel was varied within 300–700 mm Hg, argon purity was 99.999%. To obtain a rhombic 15R-SiC polytype, isovalent tin impurity (Sn) was injected into the growth zone, and the growing 6H polytype layer transformed in its presence into 15R provided that the growth was oriented in [0001] Si direction. 6H-SiC/15R-SiC heterostructures were grown, diameter of the samples was equal to ~ 15 mm, heterostructure thickness was equal to $\approx 240 \mu m$. Besides the heterostructure, 6H and 15R polytype SiC reference standards with high structural perfection and purity ($N_d - N_a \approx 5 \cdot 10^{16} cm^{-3}$) were used herein. In order to form vacancy defects, the heterostructure and reference standards were irradiated by 15 MeV protons at a rate of $6 \cdot 10^{14} cm^{-2}$ using MGTs-20 isochronous cyclotron at Peter the Great St. Petersburg Polytechnic University. It should be noted that this radiation procedure was successfully used before for formation of silicon vacancies in SiC [8,9,13]. Raman spectra and μ -PL spectra were recorded using LabRam HREvo UV-VIS-NIR-Open (Horiba, Lille, France) spectrometer equipped with a confocal microscope and a silicon CCD array cooled down to the liquid nitrogen temperature. Nd:YAG-laser (Torus, Laser Quantum, Inc., Edinburg, UK) line $\lambda = 532$ nm (2.33 eV) was used for Raman spectra and μ -PL spectra excitation. The laser beam on the sample surface was focused using Olympus 100 \times (NA = 0.9) and Leica PL FLUOTAR 50 \times (NA = 0.55) lens into a spot $\sim 1-2 \mu m$ in diameter. The spectra were recorded using 1800 and 600 gr/mm diffraction gratings. Electron paramagnetic resonance spectra were recorded using standard Jeol EPR spectrometer in X-range (≈ 9.4 GHz) at room temperature and continuous optical sample illumination by $\lambda = 808$ nm laser.

3. Results and discussion

The silicon carbide heterostructure was studied by the Raman spectroscopy method in order to identify its polytype composition. It is known that each individual SiC polytype has a typical set of acoustic and optical phonon modes [14].

The most pronounced difference between the polytypes is observed in a low-frequency Raman spectrum region where light scattering on folded transverse acoustic (FTA) phonons are recorded. This is illustrated in Figure 1, *a*, where Raman spectra recorded on 6H-SiC and 15R-SiC polytype reference standards in light scattering geometry $z(x\bar{x})\bar{z}$.

Here, z is the hexagonal optical axis direction. Frequencies corresponding to light scattering on FTA phonons are greyed out and are in accordance with the tabulated values established in [14]. Since the spectra obtained from 6H/15R heterostructure will be discussed below, Figure 1, *a* also shows an expected spectrum of such heterostructure, which was obtained by simple summation of Raman spectra for 6H-SiC and 15R-SiC polytypes.

Raman spectra measured on 6H-SiC/15R-SiC heterostructure by laser focal point scanning deep into the sample are shown in Figure 1, *b*. The upper spectrum recorded by laser focusing on the sample surface fully corresponds to 6H-SiC sample spectrum shown in Figure 1, *a*. The spectrum recorded by laser focusing deep into the sample approximately to $70 \mu m$, contains 150 and $173 cm^{-1}$ spectral lines corresponding to scattering on FTA phonons typical for 6H- and 15R-SiC polytypes, respectively. Additional line (6H/15R Interface) at $\sim 157 cm^{-1}$ in the spectrum shown in Figure 1, *b* by arrows probably occurs due to light scattering on acoustic phonons at the heterostructure interface. Further scanning at about $110 \mu m$ deep into the sample shows that only 15R-SiC polytype without foreign inclusions is present. According to the scanning results, it can be concluded that the studied heterostructure is actually 6H-SiC/15R-SiC.

Further, 6H-SiC/15R-SiC heterostructure was studied by the low-temperature confocal microphotoluminescence method. For optical spectrum interpretation, an approach similar to that used for the investigation of this heterostructure by the Raman spectroscopy method was used. More specifically, μ -PL investigations of each polytype separately were carried out on proton-irradiated 6H-SiC and 15R-SiC reference samples. The corresponding spectra with marked zero-phonon line positions of silicon vacancies designated in accordance with the nomenclature in the table are shown in Figure 2, *a*. It should be noted here that zero-phonon lines $V1$ and $V1'$ observed in 15R polytypes are not shown in the table, because they have not been discussed in the literature before. Figure 2, *b* shows the spectrum found by adding the spectra recorded separately for 6H-SiC and 15R-SiC polytypes. Finally, a general picture of the expected PL spectrum of the silicon vacancies in 6H-SiC/15R-SiC heterostructure was shown. Figure 3 shows μ -PL spectrum recorded on 6H-SiC/15R-SiC heterostructure. It can be seen that this spectrum and summarized spectrum shown in Figure 2, *b* are fully compliant with each other. Thus,

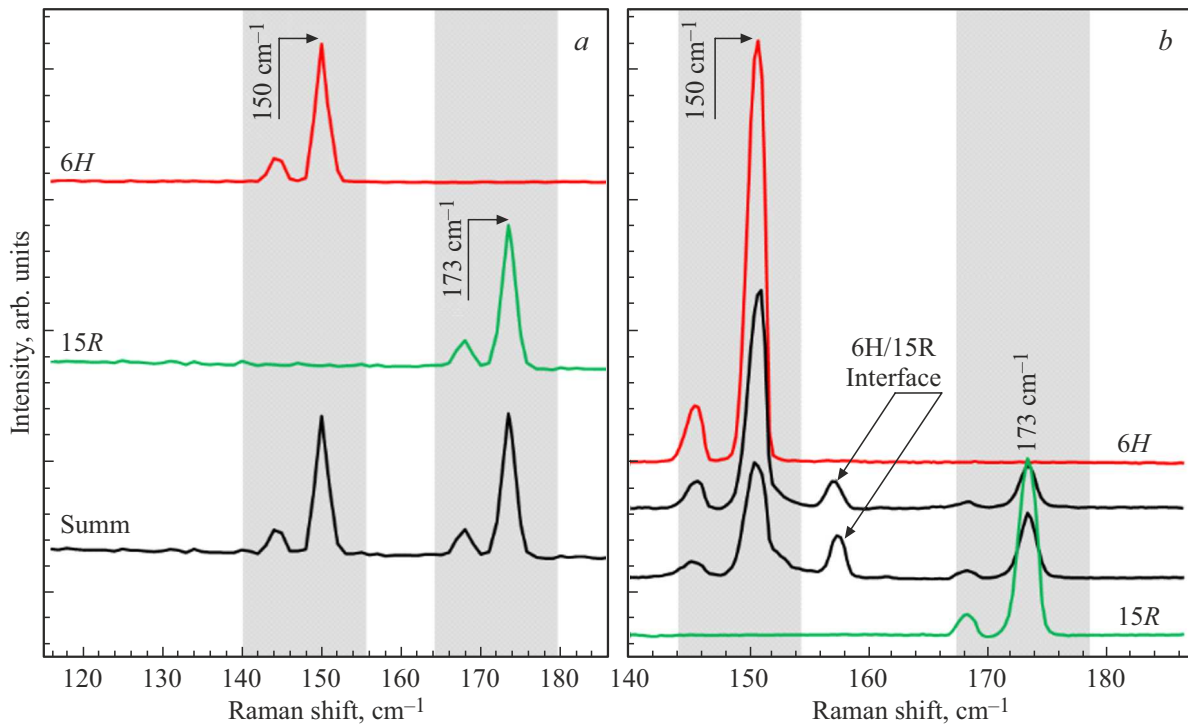


Figure 1. (a) Raman spectra recorded on 6H- and 15R-SiC polytypes at room temperature and optical excitation by $\lambda = 532$ nm laser. The lower spectrum was found by addition of 6H-SiC and 15R-SiC spectra. (b) are Raman spectra recorded on 6H/15R-SiC heterostructure by laser focal point scanning deep into the sample. The upper spectrum was recorded by laser focusing onto the sample surface. The second and third spectra correspond to the laser focal point at a heterostructure depth of 70 and 80 μm . The lower spectrum corresponds to focusing at a depth of 110 μm .

it is shown that silicon vacancies in 6H-SiC/15R-SiC heterostructures may be introduced by proton irradiation and are characterized by similar spectral set of zero-phonon lines, i.e. V_1 , V_2 , V_3 for 6H-SiC polytype, and V_1 , V_1' , V_2 , V_3 and V_4 for 15R-SiC polytype, which can be clearly seen from the zoomed-in spectra.

After spectral identification of silicon vacancies in 6H-SiC/15R-SiC heterostructure by zero-phonon photoluminescence lines, the heterostructure was examined by the electron paramagnetic resonance method to identify whether the spin properties of silicon vacancies in the heterostructure correspond to the spin properties of silicon vacancies in 6H-SiC and 15R-SiC polytypes. Specific targets included the assessment of spin sublevel splitting in the zero magnetic field and investigation of the possible occurrence of optically-induced prevailing population of spin sublevels in the main quadruplet state. To solve these problems, EPR spectra were first measured on the proton irradiated 6H-SiC and 15R-SiC reference samples with parallel orientation of persistent external magnetic field B with respect to hexagonal axis c of silicon carbide ($B \parallel c$). The measurements are shown in Figure 4. It can be seen that the EPR spectrum for each polytype is characterized by a set of doublets (shown by arrows) whose fine structure components are inverted with respect to each other. These EPR spectra have been observed before and identify

uniquely the silicon vacancies with spin $S = 3/2$ in the ground state [5,6,11,15]. In this magnetic field orientation, degrees of magnetic field splitting between the resonance fine structure components correspond to double zero-field splitting, i.e. $\Delta B = 4D/\gamma_e$, where $\gamma_e = 28$ MHz/mT is the gyromagnetic ratio. Using these tables, the EPR signals may be easily aligned with V_1 , V_2 , V_3 , V_4 vacancy centers as shown in Figure 4 using the ratio mentioned above. The EPR signal phase inversion shows that optical pumping generates prevailing population of spin states that differs greatly from the Boltzmann distribution. Optically-induced population of the spin sublevels of silicon vacancies in 6H-SiC and 15R-SiC polytypes is shown schematically in details in Figure 4.

The lower EPR spectrum in Figure 4 was recorded on 6H/15R heterostructure by optical excitation with $\lambda = 808$ nm laser. It can be seen that it has the same set of EPR signals with the same ZFS parameters as for the spectra recorded on 6H-SiC and 15R-SiC standard crystals. In other words, correspondence between the positions of lines in this EPR spectrum and in 6H-SiC and 15R-SiC spectra is observed and shown with dashed vertical lines for clarity. It should be noted that due to the use of a higher magnetic field modulation amplitude (0.5 mT), the EPR signals recorded on the heterostructure are considerably broadened compared with the signals on spectra 1 and 2

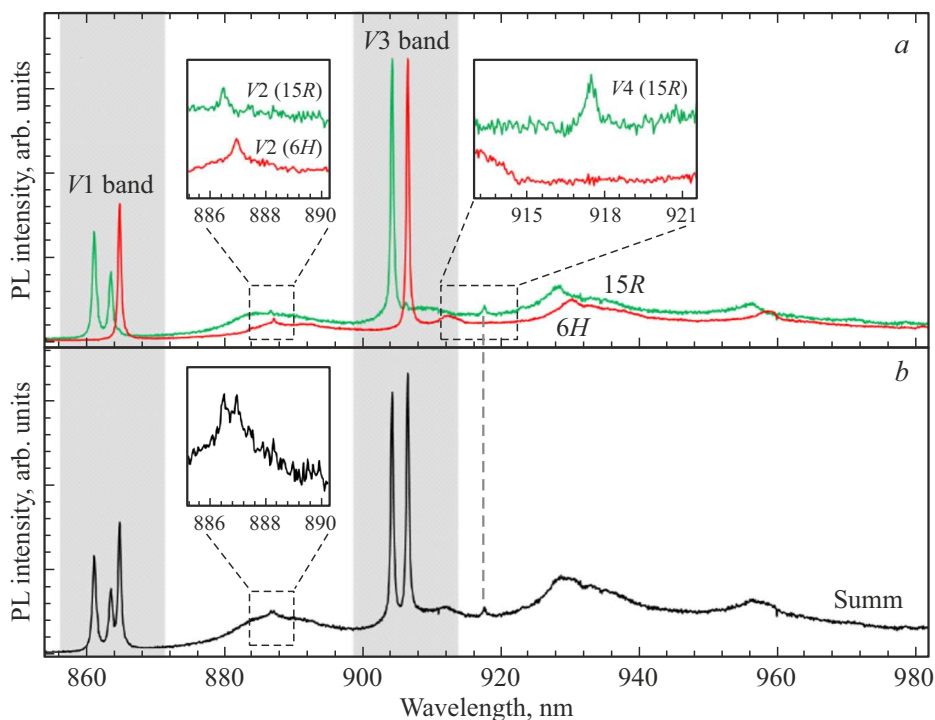


Figure 2. (a) — low-temperature ($T = 80$ K) μ -PL spectra recorded on 6H-SiC and 15R-SiC polytypes. Wavelength bands corresponding to ZPL V1/V1' and ZPL V3 (V1 band, V3 band) are greyed out. Details show zoomed-in ZPL V2 and V4 designated as V2 (6H), V2 (15R) and V4 (15R). (b) Spectrum obtained by addition of μ -PL spectra shown in Figure 1, a. The detail shows ZPL V2 position. ZPL V4 position on the summarized spectrum is shown by the dashed-dotted line.

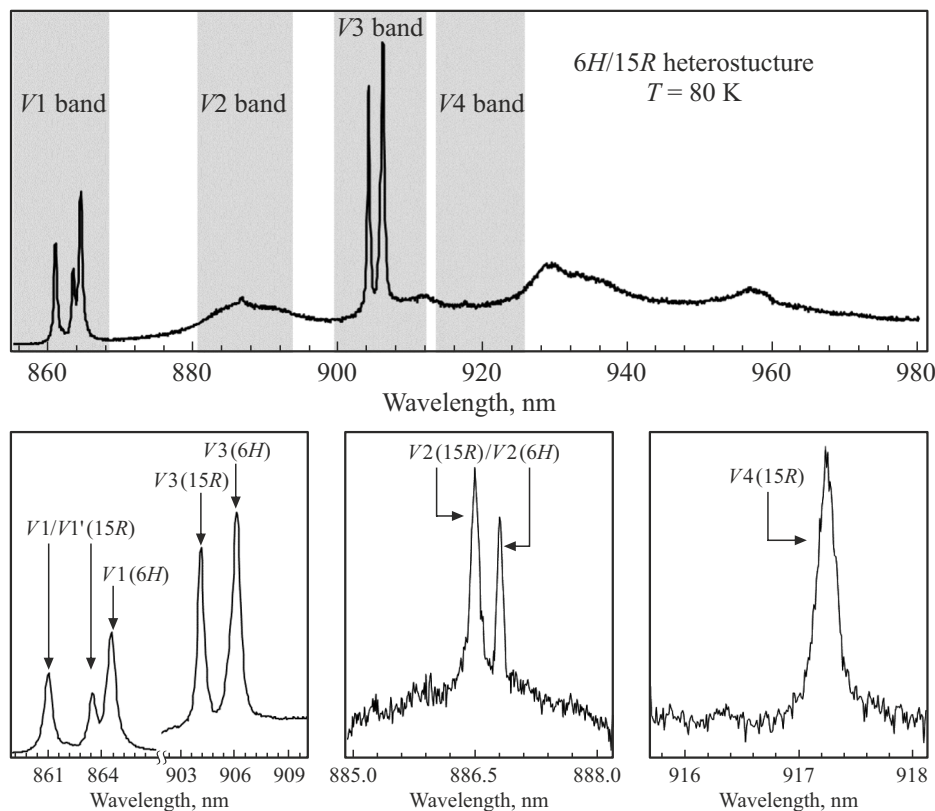


Figure 3. The upper pane shows low-temperature μ -PL spectrum recorded on 6H-SiC/15R-SiC heterostructure by broad wavelength scanning. Spectral ZPL ranges V1, V2, V3 and V4 are greyed out and their zoomed-in views are shown in the lower panes.

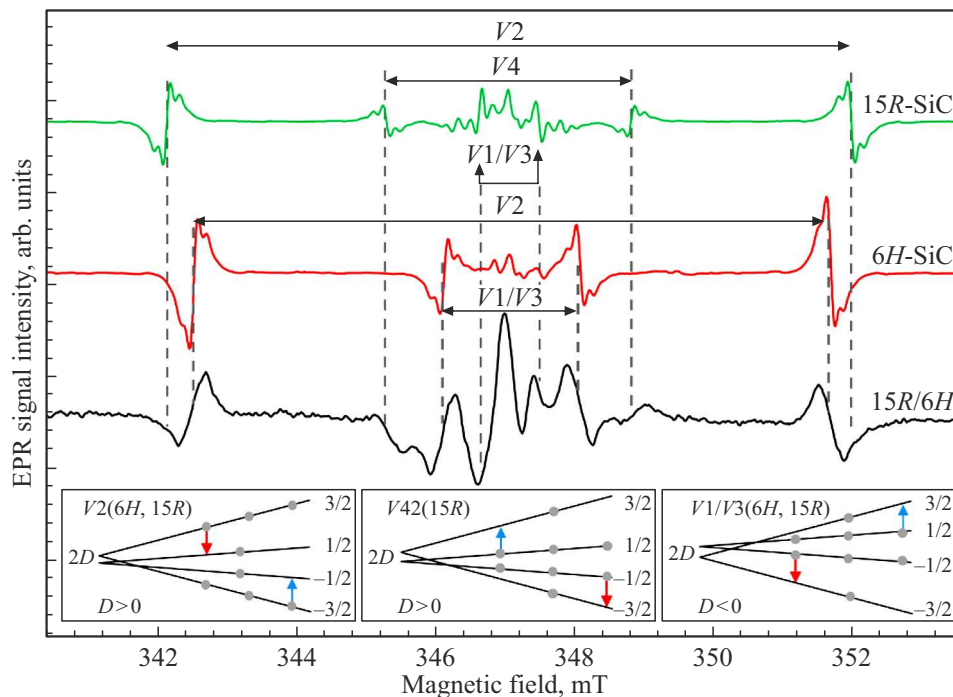


Figure 4. EPR spectra recorded on 6H- and 15R-SiC reference standards (spectra 1, 2) and on 6H-SiC/15R-SiC heterostructure (spectrum 3 with external magnetic field orientation $B \parallel c$ and optical excitation by $\lambda = 808$ nm laser. Horizontal arrows show the allowed EPR transitions ($\Delta m_s = \pm 1$). Vertical dashed lines are applied for clarity in order to emphasize the presence of all five configurations of V_{Si} centers in 6H/15R (6H ($V1/V3$, $V2$) and 15R ($V1/V3$, $V2$, $V4$)) heterostructure. Lower details show schematically optically-induced populations of spin sublevels of V_{Si} centers depending on the sign of fine structure constant D [11]. The degree of zero-field splitting (ZFS) is designated as $2D$. The arrow direction corresponds to the amplified microwave radiation/absorption.

recorded during 0.1 mT modulation. This is expressed in superposition of signals $V2$ observed in case of heterostructure. Inversion of fine structure component phases observed in spectrum 3 suggests optically-induced alignment of spin sublevels of V_{Si} centers in heterostructures. Thus, the EPR investigations clearly showed that 6H-SiC/15R-SiC heterostructure contains five spectrally resolved optically-active V_{Si} centers generated through proton irradiation.

4. Conclusion

It is shown that 6H-SiC/15R-SiC heterostructure exposure to high-energy protons results in formation of optically-active silicon vacancy centers. It has been found that optical pumping with $\lambda = 808$ nm laser causes polarization of the silicon vacancy spin sublevels in the heterostructure at room temperature. Thus, possibility of scaling up of the number of optically-active spin centers enclosed in a single crystalline matrix up to five spectrally resolved defects has been implemented. These findings enable a multi-qubit platform to be formed on the basis of such heterostructures, which is essential in terms of quantum information systems, quantum sensors and masers active at room temperature [16,17]. It has been also shown that silicon vacancy centers are the main radiation defects in proton-irradiated 6H-SiC/4H-SiC heterostructure, and this

type of irradiation does not result in macroscopic distortions of 6H- and 15R-SiC polytype crystal lattice. The latter is supported by the EPR spectroscopy, because zero-field splittings of silicon vacancy spin sublevels correspond to the values measured earlier for non-exposed samples [6]. It should be noted separately that special attention has been paid recently to spin and optical properties of vacancy defects in SiC localized in stacking faults. For example, it was shown in [18–21] that the properties of vacancy type defects located in the stacking faults differ greatly from similar defects generated in the regular environment specific to a certain SiC polytype. Modification of defect properties is associated with the fact that local short-period structural changes of SiC polytype result in the occurrence of quantum wells where a quantum confinement effect is present. Thus, the SiC heterostructures may provide an interesting possibility of investigating the properties of defects generated in the interfaces which may be addressed as a local „breakdown“ of the specified polytype resulting in the occurrence of a quantum well.

Acknowledgments

The authors express their gratitude to V.A. Soltamov for fruitful discussion of the findings.

Funding

The study was supported by RSF grant No. 22-12-00003.

Conflict of interest

The authors declare that they have no conflict of interest.

References

- [1] M.W. Doherty, N.B. Manson, P. Delaney, F. Jelezko, J. Wrachtrup, L.C.L. Hollenberg. *Phys. Rep.* **528**, 1 (2013).
- [2] D. Awschalom, R. Hanson, J. Wrachtrup, B.B. Zhou. *Nature Photon.* **12**, 516 (2018).
- [3] F.F. Murzakhonov, G.V. Mamin, S.B. Orlinskii, U. Gerstmann, W.G. Schmidt, T. Biktagirov, I. Aharonovich, A. Gottscholl, A. Sperlich, V. Dyakonov, V.A. Soltamov. *Nano Lett.* **22**, 7, 2718 (2022).
- [4] S.A. Tarasenko, A.V. Poshakinskiy, D. Simin, V.A. Soltamov, E.N. Mokhov, P.G. Baranov, V. Dyakonov, G.V. Astakhov. *Phys. Status Solidi B* **255**, 1700258 (2018).
- [5] V.S. Vainer, V.A. Il'in. *Sov. Phys. Solid State* **23**, 2126 (1981). [*Fiz. Tverd. Tela* **23**, 3659 (1981).]
- [6] P.G. Baranov, A.P. Bundakova, A.A. Soltamova, S.B. Orlinskii, I.V. Borovykh, R. Zondervan, R. Verberk, J. Schmidt. *Phys. Rev. B* **83**, 125203 (2011).
- [7] P.G. Baranov, I.V. Il'in, E.N. Mokhov, M.V. Muzafarova, S.B. Orlinskii, J. Schmidt. *JETP Lett.* **82**, 441 (2005).
- [8] H.J. von Bardeleben, J.L. Cantin, A. Csore, A. Gali, E. Rauls, U. Gerstmann. *Phys. Rev. B* **94**, 121202(R) (2016).
- [9] F.F. Murzakhonov, B.V. Yavkin, G.V. Mamin, S.B. Orlinskii, H.J. von Bardeleben, T. Biktagirov, U. Gerstmann, V.A. Soltamov. *Phys. Rev. B* **103**, 245203 (2021).
- [10] V. Ivády, J. Davidsson, N.T. Son, T. Ohshima, I.A. Abrikosov, A. Gali. *Phys. Rev. B* **96**, 161114(R) (2017).
- [11] V.A. Soltamov, B.V. Yavkin, G.V. Mamin, S.B. Orlinskii, I.D. Breev, A.P. Bundakova, R.A. Babunts, A.N. Anisimov, P.G. Baranov. *Phys. Rev. B* **104**, 125205 (2021).
- [12] Yu.A. Vodakov, E.N. Mokhov, M.G. Ramm, A.D. Roenkov. *Krist. Tech.* **14**, 729 (1979).
- [13] H.J. von Bardeleben, J.L. Cantin, I. Vickridge, G. Battistig. *Phys. Rev. B* **62**, 15 (2000).
- [14] S. Nakashima, H. Harima. *Phys. Status Solidi A* **162**, 39 (1997).
- [15] V.A. Soltamov, B.V. Yavkin, D.O. Tolmachev, R.A. Babunts, A.G. Badalyan, V.Yu. Davydov, E.N. Mokhov, I.I. Proskuryakov, S.B. Orlinskii, P.G. Baranov. *Phys. Rev. Lett.* **115**, 247602 (2015).
- [16] H. Kraus, V.A. Soltamov, D. Riedel, S. Váth, F. Fuchs, A. Sperlich, P.G. Baranov, V. Dyakonov, G.V. Astakhov. *Nature Phys.* **10**, 157 (2014).
- [17] J.D. Breeze, E. Salvadori, J. Sathian, N. McN. Alford, C.W.M. Kay. *Nature* **555**, 493 (2018).
- [18] V. Ivády, J. Davidsson, N. Deegan, A.L. Falk, P.V. Klimov, S.J. Whiteley, S.O. Hruszkewycz, M.V. Holt, F.J. Heremans, N.T. Son, D.D. Awschalom, I.A. Abrikosov, A. Gali. *Nature Commun.* **10**, 5607 (2019).
- [19] J.H. Lee, W.B. Jeon, J.S. Moon, J. Lee, S.-W. Han, Z. Bodrog, A. Gali, S.-Y. Lee, J.-H. Kim. *Nano Lett.* **21**, 9187 (2021).
- [20] N.T. Son, D. Shafizadeh, T. Ohshima, I.G. Ivanov. *J. Appl. Phys.* **132**, 025703 (2022).
- [21] H. Iwata, U. Lindefelt, S. Öberg, P.R. Briddon. *Microelectron. J.* **34**, 371 (2003).

Translated by E.Ilyinskaya